Journal of Sandwich Structures and Materials

Finite Element Analysis of Debonded Sandwich Beams Under Axial Compression

Bhavani V. Sankar and Manickam Narayanan

The online version of this article can be found at:
http://jsm.sagepub.com/cgi/content/abstract/3/3/197

Additional services and information for *Journal of Sandwich Structures and Materials* can be found at:

Email Alerts: http://jsm.sagepub.com/cgi/alerts

Subscriptions: http://jsm.sagepub.com/subscriptions

Reprints: http://www.sagepub.com/journalsReprints.nav

Permissions: http://www.sagepub.co.uk/journalsPermissions.nav

Citations http://jsm.sagepub.com/cgi/content/refs/3/3/197

Finite Element Analysis of Debonded Sandwich Beams under Axial Compression

BHAVANI V. SANKAR[*] AND MANICKAM NARAYANAN

Department of Aerospace Engineering, Mechanics and Engineering Science, University of Florida, Gainesville, FL 32611, USA

ABSTRACT: A nonlinear finite element analysis was performed to simulate axial compression of sandwich beams with debonded face sheets. The load–end-shortening diagrams were generated for a variety of specimens used in a previous experimental study. The energy release rate at the crack tip was computed using the J-integral, and plotted as a function of the load. A detailed stress analysis was performed and the critical stresses in the face sheet and the core were computed. The core was also molded as an isotropic elastic-perfectly plastic material and a nonlinear post buckling analysis was performed. A Graeco-Latin factorial plan was used to study the effects of debond length, fact sheet and core thicknesses, and core density on the load carrying capacity of the sandwich composite. It has been found that a linear buckling analysis is inadequate in determining the maximum load a debonded sandwich beam can carry. A nonlinear post-buckling analysis combined with an elasto-plastic model of the core is required to predict the compression behavior of debonded sandwich beams.

KEY WORDS: axial compression, compressive strength, crack propagation, debonding, elasto-plastic analysis, finite element analysis, Graeco-Latin factorial plan, graphite/epoxy, honeycomb core, post-buckling, sandwich composites.

INTRODUCTION

THERE IS A renewed interest in using sandwich construction in aerospace structures mainly driven by the possibility of reducing weight and cost. Fiber composites such as graphite/epoxy are favored as the face-sheet material because of their high stiffness and ability to be co-cured with many core materials. In the field of aerospace structural engineering, sandwich construction finds application in wing skins and fuselage among other structures. Debonding of the face-sheet from

*Author to whom correspondence should be addressed.

the core is a serious problem in sandwich constructions. This may occur during the fabrication process due to inadvertent introduction of foreign matter at the interface or due to severe transverse loads as in foreign object impact. The debonded sandwich panels are susceptible to buckling under inplane compressive loads, which may lead to the propagation of the delamination,[1] and/or core and face-sheet failure. Hence there is a need for a systematic study to understand how the core and face-sheet properties affect the compression behavior of a debonded sandwich composite.

There are many works concerning buckling of delaminated composite beams and plates. These models were later extended to sandwich beams. Simitses et al. (1985) and Yin et al. (1986) developed analytical models to study the effects of delamination on the ultimate load capacity of beam-plates. The latter paper included the post-buckling behavior as well as energy release rate calculations to predict delamination growth. Chen (1993) included the transverse shear effects on buckling, post-buckling and delamination growth in one-dimensional plates. A nonlinear solution method was developed by Kassapoglou (1988) for buckling and post-buckling of elliptical delaminations under compressive loads. This method employs a series solution approach in conjunction with the perturbation technique to solve the laminated plate equations for large deflections. Experiments were performed on sandwich panels containing delaminated face-sheets (note that the delaminations were in between layers of the face-sheet; the face-sheet/core interface did not contain delaminations). The nonlinear models were able to predict the onset of delamination and failure loads in the experiments.

Frostig (1992) and Frostig and Sokolinsky (1999) have developed a higher order theory for studying the buckling of delaminated sandwich panels with flexible core. Their method is capable of capturing both symmetric and anti-symmetric modes of buckling. Niu and Talreja (1999) used Winkler foundation models to study the buckling of thin debonded face layers. Minguet et al. (1987), studied the compressive failure of sandwich panels with a variety of core materials including honeycomb core. They observed three types of failure modes—core failure, debond and face-sheet fracture. Based on the test results they developed a nonlinear model to predict these failures using appropriate failure criteria for each failure mode. Sleight and Wang (1995), compared various approximate numerical techniques for predicting the buckling loads of debonded sandwich panels, and compared them with plane finite element analyses. They concluded that 2-D plane strain FE analysis is necessary in order to predict the buckling loads accurately. Hwu and Hu (1992), extended the work of Yin et al. (1986), for the case of debonded sandwich beams. They developed formulas for buckling loads in terms of sandwich beam properties and debond length. Kim and Dharan (1992), used a

---

[1]In this paper the words debonding and delamination are interchangeably used to denote the lack of bonding between one of the face sheets and the core.

beam on elastic foundation model and computed the energy release rate in debonded sandwich panels. Based on fracture mechanics they predicted critical debond lengths for crack propagation. They used their model to predict failure in plastic-foam core sandwich panels. An extensive experimental study was conducted by Kardomateas (1990), to understand the buckling and post-buckling behavior of delaminated Kevlar/epoxy laminates. The experimental program documented the load-deflection diagrams, deformation shape in post-buckling and growth of delamination.

From this literature survey it is clear that a systematic study on compression behavior of sandwich panels with debonded face-sheets, especially failure in the post-buckling regime, is overdue. Any modeling should be preceded by a testing program to understand the effects of various parameters such as face-sheet stiffness, core stiffness and core thickness, and debond length on the buckling and post-buckling behavior. In a previous experimental study (Avery, 1998; Avery and Sankar, 2000) compression tests were performed to understand the effects of core and face-sheet properties, and delamination length on the compression strength of debonded sandwich composites. A preliminary finite element analysis was presented in Avery, Narayanan and Sankar (1998).

In the present study, an attempt is being made to use finite element simulations of the compression tests to explain the failures observed in the experiments. For the purpose of completeness a brief description of the materials system used in the experiments as well as the experimental results are presented in the following section. The finite element model is described and the various possible scenarios of failure are discussed using the FE results.

EXPERIMENTAL STUDY

The sandwich composites used in the experimental study were made of graphite/epoxy face sheets and an aramid (Nomex®) honeycomb core. The face-sheet was made from Fiberite® carbon fiber/epoxy plain-woven prepregs, and the face-sheets and the core were co-cured. The honeycomb structure has orthotropic properties and its principal directions are denoted by *L*, *W*, and *t*. The *L* and *W* directions are in the plane of the core panel and the *t*-direction is the thickness direction. The properties of the face-sheet and core materials can be found in Avery (1998) and Avery and Sankar (2000). The specimens used were 4 inches long and 2 inches wide. A Teflon layer was introduced between the core and one of the face-sheets to simulate debonding. The Teflon layer covered the entire width of the specimen, and its length was varied from 0.5 inch to 2 inches.

The compression tests were conducted in a displacement controlled mode. The specimens were clamped at the ends and were subjected to axial compression. The tests were stopped after substantial load reduction due to buckling and/or catastrophic failure of the specimen. A sample compression test is illustrated by the
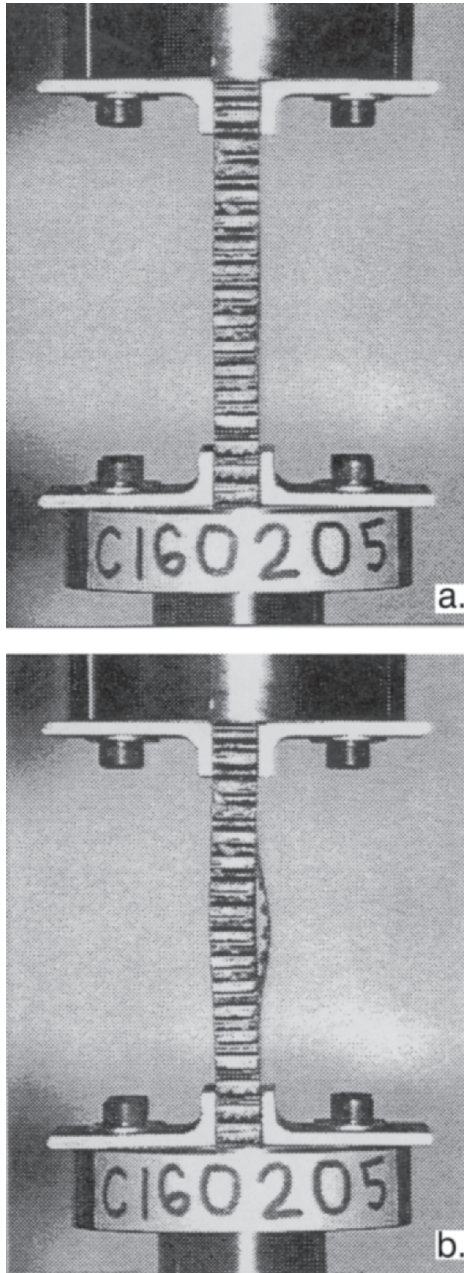
Figure 1. *A sandwich beam with debonded face sheets under axial compression. Photographs show progression of debond buckling and failure.*
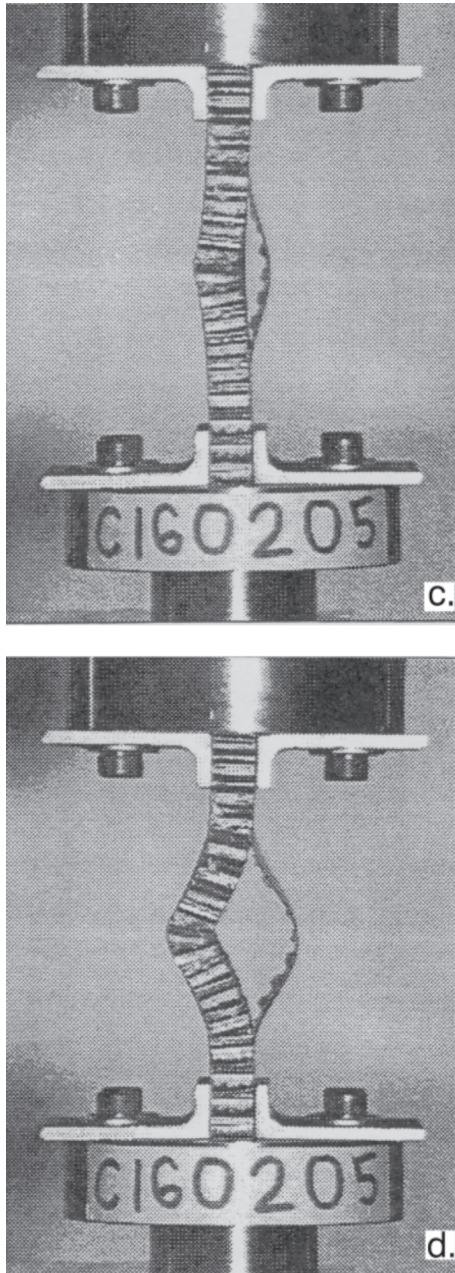
Figure 1 (continued). *A sandwich beam with debonded face sheets under axial compression. Photographs show progression of debond buckling and failure.*
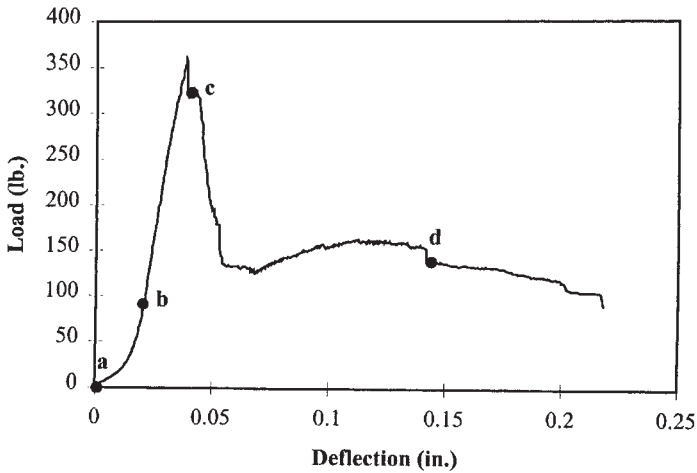
Figure 2. *Experimental load-deflection (end-shortening) diagram for the specimen shown in Figure 1.*

photographs taken at various stages of loading of one of the specimens (Figure 1). Corresponding load–end-shortening diagram is shown in Figure 2. Sixteen different types of specimens were tested to understand the effects of core thickness, core density, face sheet thickness and delamination length on the compressive load carrying capacity of the sandwich beam column. Six repeat tests were conducted for each specimen type. The specimen configuration and the maximum load at a failure for each of the sixteen tests are summarized in Table 1. The face-sheet thickness is expressed in terms of the number of plies in each face-sheet. The thickness of each ply was on the average 0.0087 inch. The failure load is given as load per unit width of the specimen (lb/in). Avery (1998) performed a Graeco-Latin Square analysis (Schenck, 1961) of the results from the sixteen specimens to understand the effects of delamination length, face sheet thickness, core thickness and core density on the failure load. The statistical analysis resulted in an empirical relation for the failure load P in terms of the test variables: a, delamination length; h, face sheet thickness; c, core thickness; and ρ, core density:

$$P = Kf_1(h)f_2(a)f_3(c)\phi(\rho) \tag{1}$$

where K is a constant and f_i and ϕ are empirical functions, which are shown in Figure 3.

In the present study, an attempt is being made to use finite element simulation of the compression tests to explain the failures observed in the experiments and to predict the maximum load a sandwich specimen with debonded face sheet can carry before failure.

Table 1. Properties of specimens used in the experimental study and their failure loads. Thickness of each fact sheet ply was about 0.0087 inch.

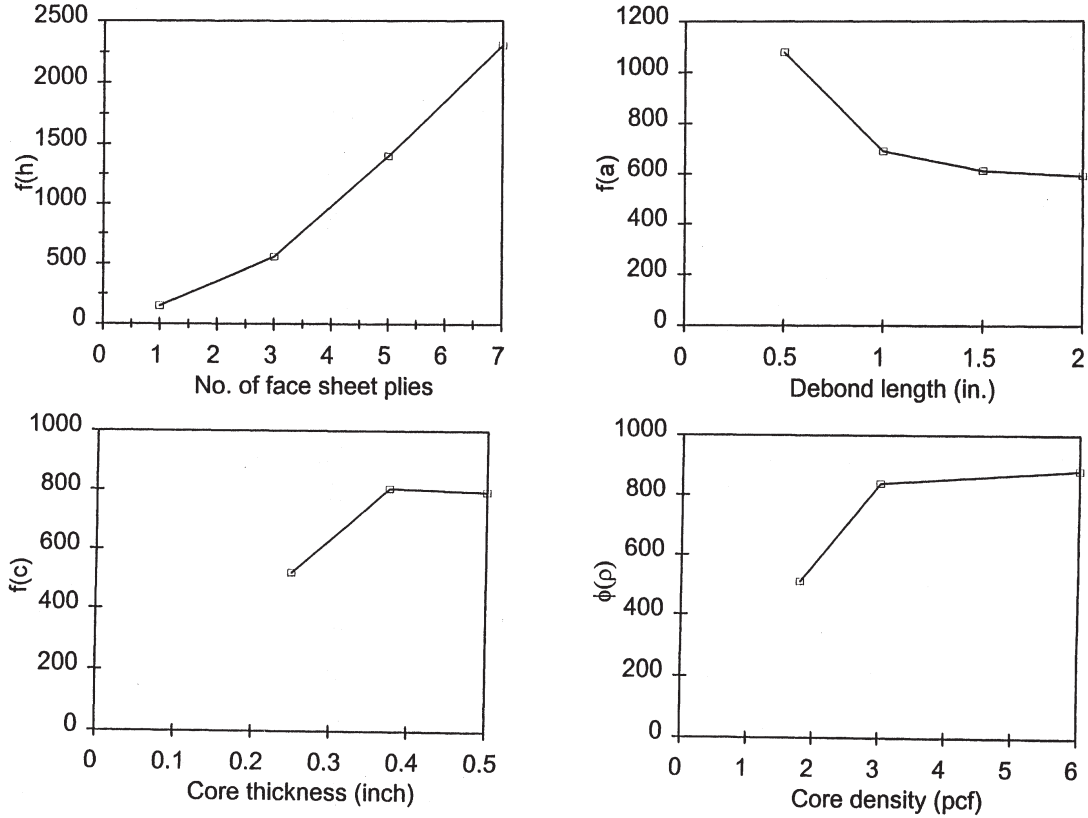| Specimen Number	Plies per Face-Sheet	Core Thickness (in)	Core Density (lb/ft^3)	Delamination Length (in)	Experimental Failure load (lb/in)
1	1	0.250	1.8	0.5	98
2	1	0.375	3.0	1.0	162
3	1	0.500	3.0	1.5	164
4	1	0.375	6.0	2.0	194
5	3	0.375	3.0	0.5	1,210
6	3	0.250	6.0	1.0	497
7	3	0.375	1.8	1.5	361
8	3	0.500	3.0	2.0	439
9	5	0.375	3.0	0.5	2,528
10	5	0.500	1.8	1.0	1,215
11	5	0.375	6.0	1.5	1,385
12	5	0.250	3.0	2.0	893
13	7	0.500	6.0	0.5	4,528
14	7	0.375	3.0	1.0	2,319
15	7	0.250	3.0	1.5	1,688
16	7	0.375	1.8	2.0	1,583

Figure 3. *Empirical relations for maximum experimental compressive load. Effects of face-sheet thickness (*h*), core thickness (*c*), debond length (*a*) and core density (*ρ*).*

FINITE ELEMENT ANALYSIS

The finite element analysis was used to estimate the linear buckling loads and mode shapes of the delaminated sandwich beams and to simulate the actual compression tests by performing a nonlinear post-buckling analysis of the sandwich beam under axial compression. The results from the linear buckling analysis are needed for the post-buckling analysis also. The FE analysis was performed using the FE package ABAQUS™ and the FE model was created using the FE pre-processor MSC/PATRAN©. The development of the FE model involved meshing of the surfaces of the geometric model and resulted in the creation of approximately 800 isoparametric elements with 2500 nodes. Since the delamination or debond was through the width of the specimen, three dimensional model was avoided, and the specimen was modeled using eight-node, biquadratic, plane strain elements. The actual width of the delamination in the experiments were 2 inches, which is very large compared to the face sheet thickness (~0.008 in). Hence, the assumption of plane strain in the width direction is justified.

The graphite/epoxy face-sheet was modeled as a homogeneous linear elastic orthotropic material throughout this study. This assumption is justified as the face-sheet did not undergo any delamination or other significant failure. The dominant failure mechanisms of interest are the core failure and the interfacial fracture. The properties used for the face-sheet and core materials are given in Table 2. The homogeneous properties of the face sheet material were derived from the data provided by the manufacturer (Fiberite™) of the plain-weave composite. The 1-direction is parallel to the longitudinal beam axis and the 2-direction is the thickness direction of the sandwich beam. A state of plane strain is considered normal to the 1-2 plane, and the beam width in the 3-direction is assumed to be unity.

Although honeycomb core was used in the experimental study, it was decided to model the core as a homogeneous continuum. This assumption is justifiable only if the characteristic dimensions of the problem are much larger than the cell size. For example, in the current problem most of the delamination lengths, except 0.5 inch, are larger than the cell size of 0.125 inch. Also, as one of the objectives was to understand the effect of core properties on the buckling and post-buckling behavior, it was decided that it was not necessary to model the microstructure of the core in detail at this stage. The core properties used in the simulations are given in Table 2. Not all properties were available from the manufacturer. For example, the transverse shear stiffness (plate shear) is available from the manufacturer. The compressive strength was obtained by Avery (1998).

The FE analyses performed can be broadly classified into two parts: Linear buckling analysis and nonlinear post-buckling analysis. The main purpose of the linear buckling analyses was to understand the effects of core thickness, core density, face-sheet thickness and delamination length on the buckling load. Further, the linear buckling mode shapes are required in specifying the imperfections

Table 2. *Properties of face-sheet and core materials used in the FE analysis. The Young's Moduli (E) and shear moduli (G) are in psi. The Poisson's ratios are denoted by ν. The core density ρ is given in pcf (lb/ft³).*

Material	E_{11}	E_{22}	E_{33}	ν_{12}	ν_{23}	ν_{31}	G_{12}	G_{23}	G_{31}
Face-sheet	7.70×10^6	1.55×10^6	7.70×10^6	0.37	0.37	0.13	0.63×10^6	0.674×10^6	0.630×10^6
Core ρ = 1.8	336	181	15,100	0.01	0.01	0.01	3,900	3,900	3,900
Core ρ = 3.0	560	302	27,000	0.01	0.01	0.01	7,000	7,000	7,000
Core ρ = 6.0	1,121	604	51,000	0.01	0.01	0.01	13,900	13,900	13,900

needed to trigger post-buckling in the nonlinear analysis. It should be mentioned that no gap elements (contact elements) were used in between the nodes on the delaminates surfaces. Thus interpenetration of the crack surfaces was not prevented in the FE analysis. However there was no interpenetration in the first buckling mode shape, and hence the use of gap elements was not pursued.

The nonlinear post-buckling analysis was performed to simulate the compression tests of the sandwich specimens. The nonlinear analysis consists of the following steps:

1. An eigen-value buckling analysis was performed on the "perfect" model to obtain the possible buckling modes.
2. In the second step of the analysis, an imperfection in the geometry was introduced by adding a fraction of deflections from the eigen modes (buckling mode shapes) to the "perfect" geometry to create a perturbed mesh. The choice of the scale factors of the various modes was dependent on the face-sheet thickness. Usually, 10% of the face-sheet thickness was assumed to be the scale factor for the major buckling mode. In the present study only the first mode shape was included in the imperfection.
3. Finally, a geometrically nonlinear load-displacement analysis of the structure was performed using the Riks method (Riks, 1979; Crisfield, 1981).

During the post buckling analyses the following quantities were computed at each load step: (a) total load and displacement (end shortening); (b) stresses σ_{xx}, σ_{yy} and τ_{xy} in the face-sheets; (c) stresses σ_{xx}, σ_{yy} and τ_{xy} in the core; and (d) J-integral around one of the crack tips.

RESULTS AND DISCUSSIONS

The FE simulations were performed on sixteen models, by varying the following parameters: face-sheet thickness, core thickness, core density and delamination length. The specimen numbers, their dimensions including the delamination length and properties correspond to those given in Table 1.

Linear Buckling Analysis

The results of the linear buckling analysis are presented in Table 3. The first buckling load P_{cr}, the experimental failure load P_{max}, and their ratios ($R = P_{max}/P_{cr}$) are given in Table 3. The last column provides a qualitative comparison of P_{max} and P_{cr}. We assume that $P_{max} \approx P_{cr}$, if $0.9 \leq R \leq 1.1$. Considering the uncertainties in the material properties, the cellular nature of the core and boundary conditions, this range for R is reasonable. Six specimens satisfy this condition. The five specimens that failed in post buckling ($R > 1.1$) have thin face sheets (1 or 3 plies) and longer delaminations. Further, when the specimens failed in

Table 3. Comparison of analytical buckling load P_{cr} and experimental failure load P_{max}. P_{max} is approximately equal to P_{cr} in six specimens, P_{max} is greater than P_{cr} in five specimens and P_{max} is less than P_{cr} in the remaining five specimens.

Specimen	P_{cr} (FEA) (lb/in)	P_{max} (Test) (lb/in)	$R = P_{max}/P_{cr}$	Comments
1	111	98	0.9	$P_{max} \approx P_{cr}$
2	32	162	5.0	$P_{max} > P_{cr}$
3	15	164	10.9	$P_{max} > P_{cr}$
4	8	194	23.0	$P_{max} > P_{cr}$
5	1,280	1,210	0.9	$P_{max} \approx P_{cr}$
6	712	497	0.7	$P_{max} < P_{cr}$
7	304	361	1.2	$P_{max} > P_{cr}$
8	193	439	2.3	$P_{max} > P_{cr}$
9	2,545	2,528	1.0	$P_{max} \approx P_{cr}$
10	1,699	1,215	0.7	$P_{max} < P_{cr}$
11	1,389	1,385	1.0	$P_{max} \approx P_{cr}$
12	789	893	1.1	$P_{max} \approx P_{cr}$
13	6,678	4,528	0.7	$P_{max} < P_{cr}$
14	3,756	2,319	0.6	$P_{max} < P_{cr}$
15	2,489	1,688	0.7	$P_{max} < P_{cr}$
16	1,647	1,583	1.0	$P_{max} \approx P_{cr}$

Table 4. Effect of increasing the delamination length from 1 to 1.2 inch in the analytical buckling loads. R is the ratio of, P_{max}, failure load in tests to P_{cr}, the analytical buckling load.

Specimen	P_{max} (Test) (lb/in)	R for a = 1 inch $R = P_{max}/P_{cr}$	P_{cr} for a = 1.1 inch (lb/in)	R for a = 1.1 inch
6	497	0.7	450	1.1
10	1,215	0.7	1,343	0.9
14	2,319	0.6	3,032	0.8

post-buckling range the failure loads were significantly higher than the buckling loads. There were five specimens that failed below the buckling load. Typically they had thicker face sheets. Three of them had 1.0 inch long delamination. In these cases the failure could be either due to other factors such as compressive failure of face sheet, e.g., specimen 13 (see Avery, 1998), or core failure.

There is another possible explanation for specimens with 1 inch delamination failing below the buckling load. From Figure 3, one can note that the failure load is sensitive to delamination length, when it is approximately equal to 1 inch. Thus, there is a possibility that the delaminations were slightly longer than one inch in the tests and this contributed to a drastic reduction in the failure load. Because of the cellular nature of the core the actual length of the delamination or the effective length of the delamination in experiments was difficult to estimate. Thus, the effective length of the delamination could be longer than the implant length and thus resulting in failure below the theoretical buckling load. In order to verify this theory buckling loads of Specimens 6, 10 and 14 were computed for 1.2 inch delamination length. The increase in 0.2 inch is arbitrary, but it is within two cell-diameters. The reduction in buckling load due to increase in delamination length and comparison with the experimental failure load are shown in Table 4. It may be noted that the *R* values have increased, and are now closer to unity.
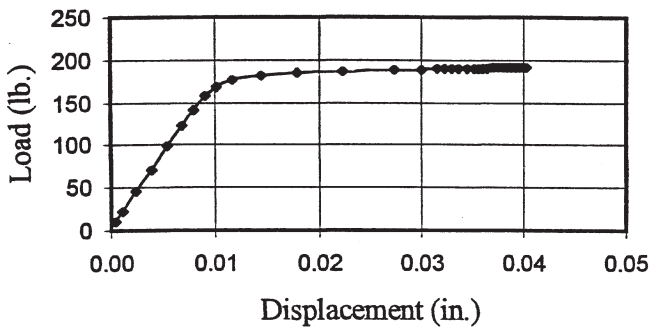

Figure 4. *Finite element simulation of a debonded sandwich beam: a sample load–end-shortening relation under post-buckling for Specimen 4.*

Post-Buckling Analysis

As mentioned before, a nonlinear analysis of the sandwich beam was performed using the Riks algorithm. The purpose of the analysis was to see if the experimental failure loads correspond to the maximum loads attained in the post buckling analysis. A sample load-deflection curve for Specimen 4 is shown in Figure 4.

The summary of maximum loads attained in the FE analysis are presented in Table 5. The FE post-buckling loads are compared to the experimental failure load by computing the ratio $R = P_{max}/P_{PB}$, where P_{PB} is the maximum load attained in the nonlinear analysis. Again it is assumed that $0.9 < R < 1.0$ indicates closer agreement between tests and simulations. From Table 5, the following observation can be made. All the specimens failed at a load approximately equal to or below the maximum load predicted by the FE post buckling analyses, i.e., R was always less than 1.1. Thus, the nonlinear FE analysis gives an upper bound for the failure load. The values are closer in eight of the sixteen specimens ($0.9 < R < 1.1$). In these specimens the delamination is generally longer, and the post buckling analysis is able to predict the load carrying capacity with reasonable accuracy. However, in other specimens the actual failure occurred at a lower load than the maximum load predicted by the finite element post-buckling analysis ($R < 0.9$), indicating that some other failure mechanisms triggered the collapse of the specimens. It should be noted that Specimen 13, which has thickest face-sheets, thickest high-density core and short delamination, has the highest post buckling load (8,100 lb/in). However, it failed at a much lower load (4,528 lb/in). This is because the face-sheets failed in compression even before the specimen went into the post buckling regime (see Avery, 1998). The maximum compressive stress in the face sheet in the FE model corresponding to the experimental failure load was found to be 54 ksi.

Energy Release Rate

From early on it was suspected that the compressive failure in a debonded sandwich beam will occur due to delamination buckling followed by catastrophic failure due to unstable delamination propagation. However, a postmortem analysis of failed specimens indicated that there was no or little crack propagation in most of the failed specimens. In order to check this, the energy release rate at the crack tip was computed using the J-integral at each load step of the post buckling analysis. A typical graph showing the variation of energy release rate with the load is presented in Figure 5. It may be seen that the energy release rate is very low until the post-buckling instability, and G rapidly raises thereafter. The energy release rate at the experimental failure load for specimens that failed below the postbuckling load is given in Table 6. In the

Table 5. Comparison of failure loads in tests and the maximum load attained in the post buckling analysis. P_{max} is approximately equal to P_{PB} in eight specimens. In the remaining eight specimens the experimental failure loads, P_{max} were below the post buckling maximum P_{PB}.

| Specimen	P_{PB} (FEA) (lb/in)	P_{max} (Test) (lb/in)	$R = P_{max}/P_{PB}$	Comments
1	91	99	1.1	$P_{max} \approx P_{PB}$
2	270	162	0.6	$P_{max} < P_{PB}$
3	330	164	0.5	$P_{max} < P_{PB}$
4	191	194	1.0	$P_{max} \approx P_{PB}$
5	1,182	1,210	1.0	$P_{max} \approx P_{PB}$
6	985	497	0.5	$P_{max} < P_{PB}$
7	430	361	0.8	$P_{max} < P_{PB}$
8	404	439	1.1	$P_{max} \approx P_{PB}$
9	3,200	2,528	0.8	$P_{max} < P_{PB}$
10	1,860	1,215	0.7	$P_{max} < P_{PB}$
11	1,406	1,385	1.0	$P_{max} \approx P_{PB}$
12	815	893	1.1	$P_{max} \approx P_{PB}$
13	8,100	4,528	0.6	$P_{max} < P_{PB}$
14	3,637	2,319	0.6	$P_{max} < P_{PB}$
15	1,744	1,688	1.0	$P_{max} \approx P_{PB}$
16	1,643	1,583	1.0	$P_{max} \approx P_{PB}$
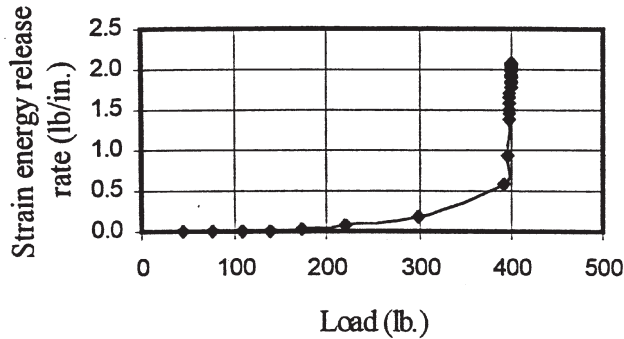
Figure 5. *Energy release rate at the crack-tip as a function of load for Specimen 8.*

same table the interfacial fracture toughness for the corresponding specimen is also given. This fracture toughness was measured using a modified sandwich DCB specimen in the experimental study (Avery, 1998). From the results it is clear that the G was considerably lower than G_c in all specimens and delamination propagation could not have been the trigger mechanism that caused the failure.

Stress Analysis

The stresses in the face sheet and the core were computed at each load step of the nonlinear analysis. A detailed mapping of stresses in most specimens can be found in Narayanan (1999). A sample plot of σ_{xx} stress distribution through the thickness of the core is presented in Figure 6. These stresses were compared with corresponding strength values to check if they could have initiated the failure. The maximum compressive stresses in the core corresponding to the experimental failure load are presented in Table 6. It must be noted that the core stresses presented in the table are values at the mid-span of the specimen. The compressive stresses near the crack tip were not analyzed as the mesh was not considered fine enough to capture the oscillating singular stress field at the crack tip. However, the mesh was good enough for computation of the J-integral.

In Table 6, the compressive strength of the core material for different specimens are also listed next to the maximum core stresses. One can note that the compressive stresses in Specimens 2 and 3 are higher than the corresponding strength values. Compressive tests on the core materials indicate that the core behaves like an elastic perfectly plastic material. Thus, the core instability could have triggered failure in some of the specimens as shown in Table 6.

Table 6. *Energy release rate at the crack tip and maximum compressive stress in the core corresponding to the experimental failure load in specimens when the specimens failed below the maximum load predicted by the post buckling analysis ($P_{max} < P_{PB}$).*

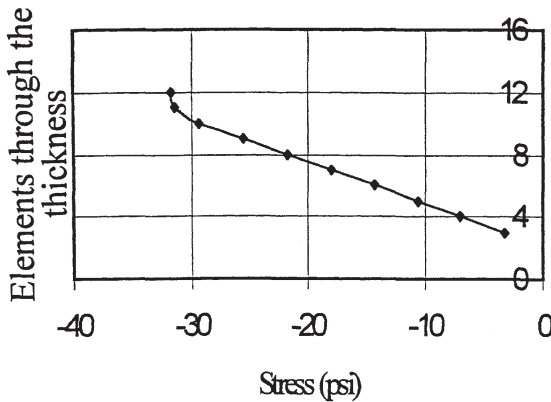| Specimen	$R = P_{max}/P_{PB}$	Energy Release Rate G (lb/in)	Fracture Toughness G_c (lb/in)	Max Core Stress (psi)	Core Compressive Strength (psi)	Possible Failure Mode
2	0.6	0.21	1.43	8.77	6.10	core
3	0.5	0.08	1.22	6.50	6.10	core
6	0.5	0.05	3.31	3.9	22.9	—
7	0.8	0.14	6.59	3.5	2.75	core
9	0.8	0.29	7.17	4.3	6.10	—
10	0.7	0.11	8.05	2.9	2.75	core
14	0.6	0.13	7.94	6.5	6.1	core

Figure 6. *Through-the-thickness* σ_{xx} *stress distribution in the core at the center of the beam in Specimen 8 for a compressive load of 391 lb/in.*

Sensitivity to Delamination Length

All specimens with one inch long delamination failed below the maximum load predicted by the post-buckling analysis. These and other specimens were analyzed with a slight increase in delamination length. The results are presented in Table 7. One can note the the postbuckling maximum was sensitive to the delamination length and an increase in delamination length brought the maximum loads closer to the experimental failure load. In spite of increasing the delamination length, the experimental failure loads of Specimens 2 ($R = 0.7$) and 3 ($R = 0.6$) are much lower than the corresponding post-buckling maximum, i.e., $R < 0.9$. Before the beam goes into post buckling instability some other failure mechanisms should have caused failure of these two specimens. Since the compressive stresses in the core were much higher than the compressive strength, it is speculated that the core became unstable and lead to collapse of the core and hence the specimen. Since the simulations used linear elastic models for the core this failure phenomenon could not have been captured.

In order to verify this concept a preliminary study was conducted wherein the core was modeled as an isotropic elastic perfectly plastic material. The isotropic behavior was due to limitations of the FE software and also due to lack of availability of orthotropic elasto-plastic properties of the core. In the isotropic model the yield strength of the core material was assumed to be 120 psi. The load-end shortening relationship for Specimen 5 is shown in Figure 7. One can note a sudden load drop at about 1000 lb which is due to the core going into the plastic regime. This trend is similar to that observed in tests (see Figure 2) by Avery (1998) and Avery and Sankar (2000). This result suggests appropriate mod-

Table 7. *Effect of increase in crack length on the maximum attained load in the nonlinear post-buckling analysis.*

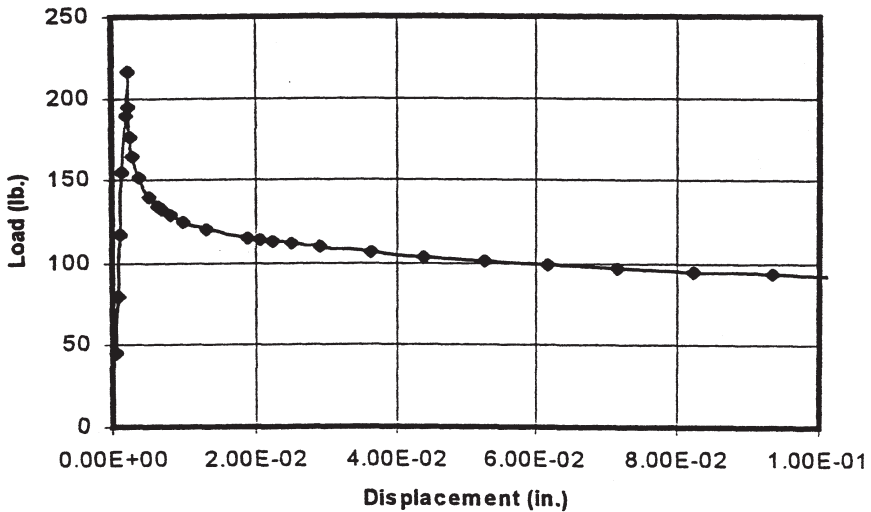| Specimen	P_{max} (Test) (lb/in)	Delamination Length a (in)	$R = P_{max}/P_{PB}$	New Crack Length a' (in)	P_{PB} for New Crack Length (lb/in)	R for Crack Length a'
2	162	1.0	0.6	1.2	226	0.7
3	164	1.5	0.5	1.7	266	0.6
6	497	1.0	0.5	1.2	605	0.8
7	361	1.5	0.8	1.6	360	1.0
9	2,528	0.5	0.8	0.6	2,122	1.2
10	1,215	1.0	0.7	1.2	1,500	0.8
14	2,319	1.0	0.6	1.2	2,700	0.9

Figure 7. *Finite element load–end-shortening curve for Specimen 5 with core modeled as an elastic-perfectly plastic material.*

eling of the elasto-plastic behavior of the core is important in predicting the behavior of debonded sandwich beams.

Parametric Studies

A Graeco-Latin Square Factorial Scheme (Schenck, 1961) was devised to isolate the effects of various parameter on the maximum post-buckling load P_{PB} obtained in the FE analysis with linear elastic core properties. This method of studying the effects of different variables on the objective function is very similar to the one Avery (1998) performed on his experimental failure loads. An empirical formula similar to that in Equation (1) was derived for the maximum post-buckling load. The effects of various parameters on the post-buckling maximum load P_{PB} are shown in Figure 8. One can note that similarities between the empirical relations presented in Figure 8 for the FE results and in Figure 3 for the experimental results. The major difference is in $f(a)$, the functional relationship between maximum load and delamination length. In experiments the maximum load drops drastically between 0.5 and 1.0 inch delamination, and then decreases slowly with increase in delamination length (see Figure 3). However, the FE model predicts drastic reduction between 1 and 1.5 inches (see Figure 8). As explained earlier the reasons for this discrepancy could be slightly longer delamination in tests and core failure in the tests.
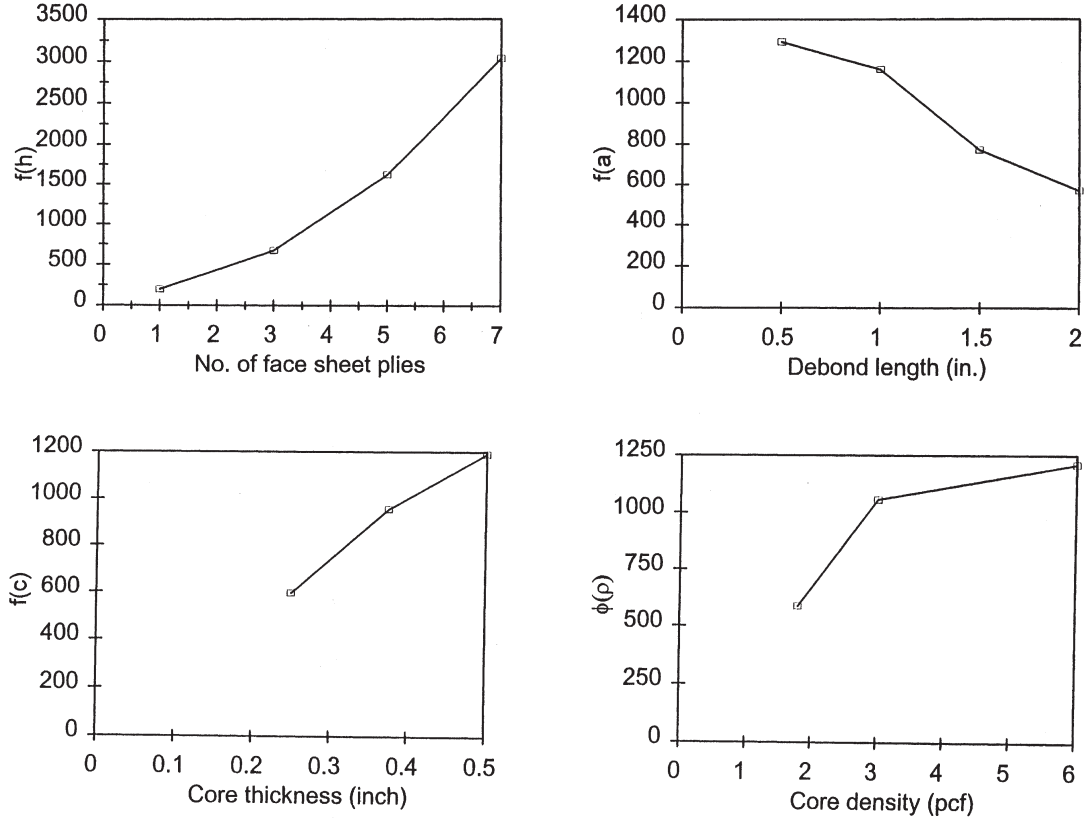
Figure 8. *Empirical relations for maximum compressive load predicted by nonlinear FE analysis. Effects of face-sheet thickness (*h*), core thickness (*c*), debond length (*a*) and core density (*ρ*).*

CONCLUSIONS AND FUTURE WORK

A finite element analysis was performed to simulate axial compression of debonded sandwich beams. Eight node plane strain elements were used to model the face-sheets and the core. A linear buckling analysis was performed to determine the buckling loads and corresponding mode shapes. The nonlinear analysis modeled the post buckling behavior of the sandwich beams. The load–end-shortening diagrams were generated for a variety of specimens used in a previous experimental study. The energy release rate at the crack tip was computed using the J-integral, and plotted as a function the load. A detailed stress analysis was performed and the critical stresses in the face sheet and the core were computed. The core was also modeled as an elastic-perfectly plastic material and the nonlinear post buckling analysis was performed.

By comparing the experimental failure load and the FEA results the following conclusions can be reached. The linear buckling analysis is inadequate in predicting the load carrying capacity of debonded sandwich beams. Thus a nonlinear post-buckling analysis is required to predict the compression behavior. The maximum load attained in the post-buckling analysis corresponds to the experimentally determined compressive strength in 50% of the specimens. These are, typically, specimens containing long disbonds (1.5 or 2.0 inches). As the load is increased these specimens become unstable, and the stresses and energy release rate at the crack-tip raise rapidly causing catastrophic failure. In the remaining 50% of the specimens failure occurred before the maximum load predicted by the post-buckling analysis. These are specimens with short disbonds (0.5 and 1.0 inch). The energy release rate was considerably lower than the interfacial fracture toughness thus eliminating interface failure as a mechanism for the specimen failure. It was found that the maximum load is very sensitive to the delamination length when it is about 1 inch. A slight increase in delamination length drastically reduces the failure load both in experiments and analysis. The stress analysis results show that the in specimens with short disbonds compressive stresses in the core exceeded the compressive strength indicating that core failure could have triggered the specimen failure. A preliminary study was conducted wherein the core was modeled as an isotropic elastic-perfectly plastic material. There was a sharp load drop as the specimen was loaded, and this behavior was similar to the experimental observations.

In conclusion a nonlinear post-buckling analysis is adequate for sandwich beams containing long disbonds. To obtain a conservative estimate of the compressive strength a slightly longer delamination should be considered. The increase in the debond length could be as much as one cell diameter. When the delaminations are short, core failure can trigger the instability, and hence the elasto-plastic behavior of the core should be included in the model in order to predict the compressive load carrying capacity of debonded sandwich beams.

ACKNOWLEDGMENTS

REFERENCES

Avery, J. L., 1998. "Compressive Failure of Delaminated Sandwich Composites," Master of Science thesis, Department of Aerospace Engineering, Mechanics & Engineering Science, University of Florida, Gainesville, Florida.

Avery, J. L., Narayanan, M. and Sankar B.V., 1998. "Compressive failure of debonded sandwich beams," *Recent Advances in Mechanics of Aerospace Structures and Materials,* Sankar, B.V. (Editor), American Society of Mechanical Engineers, New York, pp. 207–217.

Avery, J. L. and B. V. Sankar, 2000. "An experimental study of post-buckling behavior of debonded sandwich composites," *J. Composite Materials,* 34(14):1176–1199.

Chen, H. P., 1993. "Transverse Shear Effects on Buckling and Postbuckling of Laminated and Delaminated Plates," *AIAA Journal,* 31(1): 163–169

Crisfield, M. A. (1981). "A fast incremental/iterative solution procedure that handles snapthrough," *Computers & Structures,* 13:55–62.

Frostig, Y., 1992, "Behavior of delaminated sandwich beams with transversely flexible core–Higher Order Theory," *Composite Structures,* 20:1–16.

Frostig, Y. and Sokolinsky, V., 1999, "Buckling of debonded (delaminated) sandwich panels with a transversely flexible core," *Advances in Aerospace Materials and Structures,* Newaz, G. (Editor), American Society of Mechanical Engineers, New York, pp. 23–40.

Hwu, C. and J. S. Hu. 1992. "Buckling and Postbuckling of Delaminated Composite Sandwich Beams," *AIAA Journal,* 30(7):1901–1909.

Kardomateas, G. A. 1990. "Postbuckling Characteristics in Delaminated Kevlar/Epoxy laminates: An Experimental Study. *J. Composites Technology & Research,* 12(2): 85–90.

Kassapoglou, C. 1988. "Buckling, Post-Buckling and Failure of Elliptical Delaminations in Laminates under Compression," *Composite Structures,* 19:139–159.

Kim, W. C. and C. K. H. Dharan, 1992. "Face-sheet debonding criteria for composite sandwich panels under in-plane compression," *Engineering Fracture Mechanics,* 42(4):642–652.

Minguet, P., J. Dugundji and P. A. Lagace, (1987). "Buckling and Failure of Sandwich Plates with Graphite-Epoxy Faces and Various Cores," *J. Aircraft,* 25(4):372–379.

Narayanan, M. 1999. *Finite Element Analysis of Debonded Sandwich Beams Under Compression,* Master of Science Thesis, University of Florida, Gainesville, FL, December 1999.

Niu, K. and Talreja, R., 1999, "Buckling of a thin face layer on Winkler Foundation with debonds," *J. Sandwich Structures and Materials,* 1(4):259–278.

Riks, E. (1979). "An incremental approach to the solution of snapping and buckling problems," *J. Solids. Struct.* 15:529–551.

Schenck, H. (1961), *Theories of Engineering Experimentation,* McGraw-Hill, New York, NY, pp. 85–115.

Simitses, G. J., S. Sallam and W. L. Yin, 1985. "Effect of Delamination of Axially Loaded Homogeneous Laminated Plates," *AIAA Journal,* 23(9): 1437–1444.

Sleight, D. W. and J. T. Wang, 1995. "Buckling Analysis of Debonded Sandwich Panel Under Compression," *NASA Tech Memorandum 4701.*

Yin, W.-L., S. N. Sallam and G. J. Simitses, 1986. "Ultimate Axial Load Capacity of a Delaminated Beam-Plate," *AIAA Journal,* 24(1):123–128.